Applied Catalysis B: Environmental 303 (2022) 120906

Contents lists available at ScienceDirect

Applied Catalysis B: Environmental

journal homepage: www.elsevier.com/locate/apcatb

Capsule-like zeolite catalyst fabricated by solvent-free strategy for para-Xylene formation from CO_2 hydrogenation

Weizhe Gao [a], Lisheng Guo [b,*], Qinming Wu [c], Chengwei Wang [a], Xiaoyu Guo [a], Yingluo He [a], Peipei Zhang [a], Guohui Yang [a], Guangbo Liu [d], Jinhu Wu [d], Noritatsu Tsubaki [a,*]

[a] Department of Applied Chemistry, School of Engineering, University of Toyama, Gofuku 3190, Toyama 930–8555, Japan
[b] School of Chemistry and Chemical Engineering, Anhui University, Hefei, Anhui 230061, China
[c] Key Lab of Applied Chemistry of Zhejiang Province and Department of Chemistry, Zhejiang University, Hangzhou 310007, China
[d] Qingdao Institute of Bioenergy and Bioprocess Technology, Chinese Academy of Sciences, Qingdao 266101, China

ARTICLE INFO

Keywords:
Solvent-free synthesis
HZSM-5 @Silicalite-1 core-shell zeolite
CO_2 conversion
Aromatics
Para-Xylene

ABSTRACT

An efficient Na-FeMn/HZSM-5@Silicalite-1 catalyst was rationally designed for direct conversion of CO_2 to aromatics. The tailor-made HZSM-5@Silicalite-1 core-shell zeolite was prepared by a facile solvent-free method. The solvent-free synthesis of core-shell zeolite could not only address pollution issues by eliminating the large utilization of organic reagents, but also exhibit a better performance for separating para-Xylene (PX) from xylenes with the assistance of capsule-like zeolite oriented synthesis. For CO_2 to aromatics reaction, Na-FeMn combining with capsule-like HZSM-5@Silicalite-1 catalyst could reach 81.1% PX/X (the C-mol ratio of PX to all xylenes) ratio, which was higher than those of conventional core-shell zeolites, such as HZSM-5@SiO_2 and HZSM-5@Silicalite-1 core-shell zeolites which were obtained from traditional chemical liquid deposition and hydrothermal methods. The as-synthesized zeolite paves a new route for efficient conversion of CO_2 molecules into valuable PX, and provides a facile method for regulating surface acid properties of zeolite.

1. Introduction

In the past decades, the rapid rise of carbon dioxide (CO_2) concentration in the atmosphere leads to some serious issues for environment such as global warming, ocean acidification, and so on [1–6]. The direct transformation of CO_2 to high value-added chemicals has attracted much attention [7–10]. It not only partially relieves the emission of CO_2, but also effectively creates benefits [11,12]. Among all of these strategies for CO_2 conversion, there is no doubt that Fischer-Tropsch synthesis (FTS) is the most powerful route, which permits direct transformation of CO_2 into economically valuable hydrocarbons, such as gasoline, olefins, and aromatics [13–17]. In terms of FTS route, CO_2 is firstly transformed into CO by the reverse water-gas shift (RWGS) reaction and then the formed CO is subsequently converted to olefins or aromatics [18–20]. However, the produced hydrocarbons follow the Anderson-Schulz-Flory (ASF) distribution law [21]. To break the ASF distribution and increase the selectivity of target product, rational design of highly efficient catalysts via a series of strategies has been investigated extensively.

Aromatics, especially BTX (benzene, toluene and xylenes), are the most basic chemicals for the polymer industry [22,23]. In particular, para-Xylene (PX) synthesis has drawn wide attention due to the fact that it is an important raw chemical for producing terephthalic acid and PET plastics [24,25]. Generally, PX is mainly produced from the petroleum hydrocracking [26,27]. However, the production of PX from the decreasing petroleum resources cannot meet the growing demand annually in the world [24]. Therefore, it is urgent to develop some alternative non-petroleum routes for producing PX.

In recent years, direct conversion of CO_2 to aromatics via a FTS route by utilizing a composite catalyst containing iron and zeolite catalysts has attracted intensive attention [28–30]. In this process, C_nH_{2n} species are firstly formed over Fe-based catalyst and then transformed into aromatics with the assistance of ZSM-5 zeolite catalyst through aromatization reaction [31]. For the production of target PX product in real reaction system, it is firstly formed within the micropores of ZSM-5 zeolite and simultaneously isomerized to other isomers or alkylated to heavy aromatics over the external surface during the diffusion process, in consideration of the external surface Brønsted acid sites and the thermodynamics effect [8,32]. In order to enhance PX selectivity, it is

* Corresponding authors.
E-mail addresses: lsguo@ahu.edu.cn (L. Guo), tsubaki@eng.u-toyama.ac.jp (N. Tsubaki).

https://doi.org/10.1016/j.apcatb.2021.120906
Received 22 September 2021; Received in revised form 1 November 2021; Accepted 4 November 2021
Available online 9 November 2021

crucial to eliminate the external surface Brønsted acidity of ZSM-5 zeolite. To solve this problem, several methods have been developed such as inert SiO_2 deposition, non-acidic Silicalite-1 shell encapsulation, and so on [33,34]. For example, Cui et al. fabricated a catalyst composing of ZnFeOx-nNa and HZSM-5, achieving 75.6% aromatics selectivity in all hydrocarbons for CO_2 conversion [31]. Furthermore, after coating HZSM-5 zeolite by SiO_2 shell, the fraction of PX in xylenes was apparently increased from 56% to 75% [31]. Wang et al. designed a bifunctional catalyst composing of Cr_2O_3 and ZSM-5 zeolite for CO_2 conversion, exhibiting 76% aromatics selectivity [35]. Thereinto, the fraction of PX in xylenes was increased from 68.5% to 71.7% by encapsulating the ZSM-5 with Silicalite-1 zeolite shell [35]. Compared with SiO_2 shell, the Silicalite-1 zeolite shell is more promising for separating PX from other xylenes due to the unique shape selectivity (MFI type zeolite). As a consequence, constructing a ZSM-5@Silicalite-1 core-shell zeolite is one of the key steps for efficiently converting CO_2 molecules into valuable PX. Typically, the ZSM-5@Silicalite-1 core-shell zeolite was prepared by environmentally unfriendly hydrothermal method, in which large amounts of organic solvents were employed and a large amount of wastewater was formed [24,35].

For green and sustainable synthesis of zeolite, there is no doubt that the solvent-free method is the most promising strategy [36]. This method by grinding and heating the solid raw materials, can significantly avoid the production of wastewater and increase the yield of zeolite [37–39]. In 2012, Ren et al. successfully synthesized ZSM-5 or Silicalite-1 zeolite by mechanically mixing the solid raw materials [40]. Based on the above inspiration, it is possible to directly synthesize the ZSM-5@Silicalite-1 core-shell zeolite by a solvent-free method.

In this work, a composite catalyst was designed for direct conversion of CO_2 to aromatics, composing of Na-FeMn catalyst and HZSM-5 zeolite. The 36.5% aromatics selectivity at the CO_2 conversion of 27.0% was achieved at a single-pass process. At the same time, the PX/X (the C-mol ratio of PX to all xylenes) ratio was sharply increased from 51.0% to 81.1%, when the HZSM-5 zeolite was encapsulated Silicalite-1 zeolite by the solvent-free method. The external surface acidity of HZSM-5 zeolite could be effectively passivated in the presence of Silicalite-1 zeolite shell. Compared with other common core-shell zeolites, such as HZSM-5@SiO_2 and HZSM-5@Silicalite-1 obtained from conventional chemical liquid deposition and hydrothermal methods, the well-designed HZSM-5@Silicalite-1 core-shell zeolite synthesized via the solvent-free method exhibited higher PX/X ratio.

2. Experimental

2.1. Catalyst preparation

The Fe and FeMn (Fe/Mn molar ratios were 95/5, 90/10 and 80/20) catalysts were prepared by a precipitation method. In brief, Fe$(NO_3)_3$•$9H_2O$ and Mn$(NO_3)_2$•$6H_2O$ were dissolved in deionized water, and Na_2CO_3 as a precipitant was dissolved in deionized water. The two aqueous solutions were dropwise added into one beaker under agitation, controlling the temperature and pH at 75 °C and 7.0, respectively. After 1 h static aging at the same temperature, the precipitates were washed by distilled water until PH = 7.0 and collected by filtration. The solid was dried overnight at 120 °C and calcined at 500 °C for 5 h. The obtained catalysts were denoted as FeMn (x/y).

Sodium modified Fe and FeMn (x/y) catalysts with different n wt% Na loading (n = 1–7 wt% based on ICP analysis) were prepared by an impregnation method. Typically, the Na_2CO_3 solutions with different concentrations were dropwise added into the Fe or FeMn (x/y) catalyst. Subsequently, it was dried overnight at 120 °C and calcined at 500 °C for 5 h. The obtained catalysts were denoted as nNa-Fe and nNa-FeMn (x/y).

HZSM-5 zeolite samples with different SiO_2/Al_2O_3 ratio (24, 40, 105, 300 or 1500) were purchased from Mizusawa Industrial Chemicals Co. Ltd.

HZSM-5@Silicalite-1 core-shell zeolite samples were prepared by solvent-free and hydrothermal methods, respectively. For the solvent-free method, 5 g HZSM-5 zeolite, 2.23 g TPAOH (40 wt%) and 4 g fumed silica were mixed together. After finely grinding 2 h, the mixture was transferred to an autoclave and maintained at 180 °C for 72 h. This synthesis process was conducted twice. The HZSM-5@Silicalite-1 core-shell zeolite (solvent-free method) was obtained after filtrating with distilled water, then drying at 120 °C and calcining at 550 °C for 5 h. The as-synthesized sample was denoted as HZSM-5@S1-S. For the hydrothermal method, 1 g HZSM-5 zeolite, 0.3 g TPAOH (40 wt%), 0.8 g fumed silica, 7.52 g EtOH and 43 g H_2O were mixed. After stirring for 4 h, the mixture was transferred to an autoclave and maintained at 180 °C for 24 h. The synthesis process was repeated twice. The HZSM-5@Silicalite-1 core-shell zeolite (hydrothermal method) was obtained after filtrating with distilled water, then drying at 120 °C and calcining at 550 °C for 5 h. The sample was marked as HZSM-5@S1-H.

HZSM-5@SiO_2 core-shell zeolite sample was prepared by a chemical liquid deposition (CLD) method. Firstly, 1 g HZSM-5 was immersed into 7 g n-hexane. Subsequently, 2 g Tetraethoxysilane (TEOS) was dropwise added into the mixture. After stirring for 4 h, the mixture temperature was increased from room temperature to 80 °C for evaporating the n-hexane. The HZSM-5@SiO_2 core-shell zeolite was obtained after calcining at 550 °C for 5 h. The synthesis process was conducted twice.

2.2. Catalyst characterization

XRD patterns of the catalysts were obtained with a Rigaku RINT 2400 system diffractometer by employing Cu-Kα (40 kV, 40 mA) radiation at room temperature.

H_2 temperature-programmed reduction (H_2-TPR) profiles were recorded by a BELCAT-B-TT catalyst analyzer equipped with thermal conductive detector (TCD). 50 mg catalyst was pretreated at 150 °C for 1 h under a flow of pure He to remove the physical adsorption of water, and then followed by temperature programmed reduction in H_2 from 40 to 700 °C with a heating rate of 10 °C min^{-1}.

The Na content of modified Fe-based catalysts was determined by an ICP atomic emission spectrometry (PROFILE SPEC).

X-ray photoelectron spectroscopy (XPS) spectra were carried out using a Thermo Fisher Scientific ESCALAB 250Xi multifunctional spectroscopy equipped by an in situ reduction pretreatment chamber.

The surface area, micropore volume and pore size of zeolite samples were collected by N_2 physical adsorption on a Micromeritics 3Flex 2MP instrument. Before sample analysis, the samples were degassed at 200 °C for 4 h.

^{27}Al NMR spectra were recorded on a Bruker Avance IIITM at 400 MHz.

NH_3 temperature-programmed desorption (NH_3-TPD) profiles were measured by a BELCAT-B-TT catalyst analyzer equipped with thermal conductive detector (TCD). Firstly, the 50 mg sample was pretreated at 500 °C for 1 h under a flow of pure He. After cooling down to 50 °C, the sample was saturated with NH_3. Subsequently, He was employed to remove the physically adsorbed NH_3 at the same temperature. Finally, the temperature was performed from 50 to 800 °C with a heating rate of 10 °C min^{-1} under a flow of He.

CO_2 temperature-programmed desorption (CO_2-TPD) profiles were measured by a BELCAT-B-TT catalyst analyzer equipped with thermal conductive detector (TCD). The samples were pretreated at 400 °C for 2 h under a flow of pure H_2 and saturated in CO_2 at 50 °C, and other experimental procedures are similar to those of NH_3- TPD.

Pyridine (Py) and 2,6-di-tert-butylpridine (DTBPy) adsorbed FTIR spectra were performed with a Bruker Tensor 27 FTIR spectrometer. Firstly, the zeolite sample was pressed into a thin wafer. After degassing at 450 °C and 1×10^{-2} Pa for 2 h, the wafer was exposed in the Py or DTBPy vapor for probing molecule adsorption (150 °C, 30 min). Then the FTIR spectra were recorded after evacuation at 150 °C for 30 min

Scanning electron microscopy (SEM) images were observed by JEOL JSM-6360LV equipped with JED-2300 energy dispersive spectroscopy

(EDS) attachment.

Transmission electron microscopy (TEM) for as-prepared catalysts was obtained using TOPCON-002B apparatus.

2.3. Catalytic test

The catalytic performance tests for CO_2 hydrogenation were performed on a high pressure fixed-bed steel reactor (internal diameter 6 mm). Before reaction, all catalysts were pretreated at 400 °C for 8 h with pure H_2 (40 mL min^{-1}, atmospheric pressure). After cooling down to room temperature, feed gas (25.7 vol% CO_2, 4.02 vol% Ar, and H_2 balance) was fed into the reactor. The typical reaction pressure and temperature were 3.0 MPa and 320 °C, respectively. Between the reactor and back pressure, the ice trap was employed to collect liquid products. The reaction effluents were quantitatively analyzed online with two gas chromatographs (GC-8A, Shimadzu), where one was equipped with TCD and active charcoal column for Ar, CO, CH_4, and CO_2 analysis, while another was equipped with flame ionization detector (FID) and Porapak-Q column for light hydrocarbons analysis. Two off-line gas chromatographs (GC-2014, Shimadzu) equipped with FID were employed for heavy hydrocarbons analysis. One with DB-1 column was used to analyze the heavy hydrocarbons and another with HP-INNOWAX was employed to further identify the xylene isomers in the collected liquid products. The carbon balance data of all catalysts were between 95% and 105%.

3. Results and discussion

3.1. Characterization of nNa-FeMn (x/y) catalysts

The XRD patterns of the as-prepared 1.20Na-Fe, 1.18Na-FeMn (95/5), 1.28Na-FeMn (90/10), and 1.23Na-FeMn (80/20) were shown in

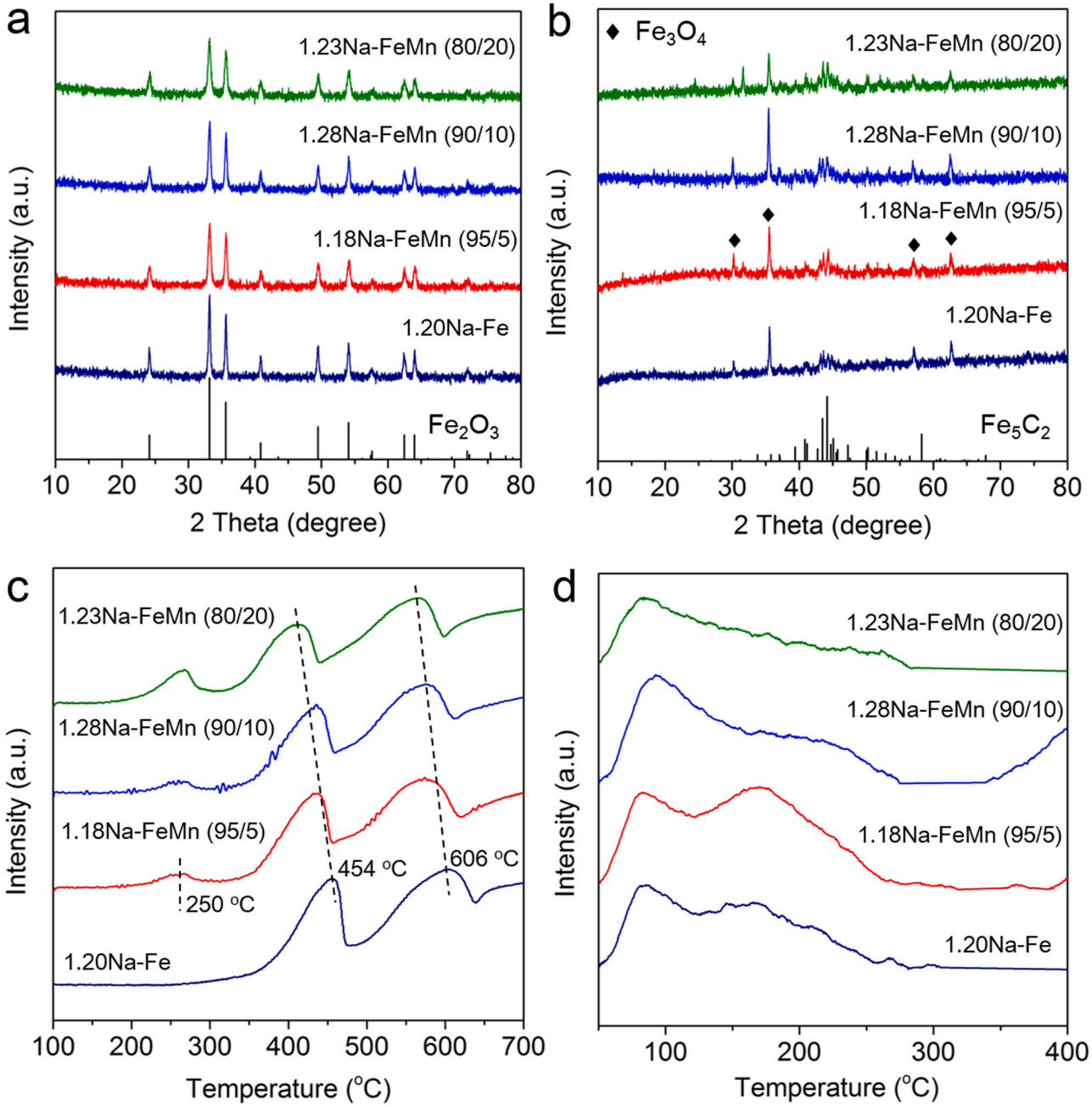

Fig. 1. (a) XRD patterns of as-prepared catalysts, (b) XRD patterns of spent catalysts, (c) H_2-TPR and (d) CO_2-TPD of Na-FeMn (x/y) catalysts.

Fig. 1a. All catalysts exhibited the characteristic peaks associated with the Fe_2O_3 phase (PDF#33–0664), while no peaks belonging to Mn oxides were detected due to the good dispersion of Mn over the Fe_2O_3 phase. After CO_2 hydrogenation reaction, the XRD patterns of spent catalysts was shown in Fig. 1b, the reflection peaks could be attributed to Fe_3O_4 (PDF#19–0629) and Fe_5C_2 (PDF#36–1248) phases. It has been proved that CO_2 is firstly transformed into CO by the RWGS reaction over Fe_3O_4, and subsequently the formed CO is converted to olefins via FTS on active carbides such as Fe_7C_3 and Fe_5C_2. H_2-TPR profile of the 1.20Na-Fe displayed two H_2 consumption peaks at around 454 and 606 °C in Fig. 1c, which were ascribed to the reduction of Fe_2O_3 to Fe_3O_4 and Fe_3O_4 to FeO, respectively. When Mn was added into the Fe-based catalyst, a new H_2 consumption peak appeared at around 250 °C, which was ascribed to the reduction of Mn_2O_3 to MnO. Moreover, further increasing the ratio of Mn in FeMn samples from 95/5 to 80/20 (Fe/Mn molar ratio), the reduction peaks of Fe oxides generally shifted to lower temperature, indicating that the addition of Mn facilitated the reduction of Fe oxides. The CO_2-TPD profiles of as-prepared catalysts were also presented in Fig. 1d. The lower temperature peak at around 170 °C was corresponded to the weakly adsorbed CO_2 on the surface of catalyst. Obviously, the adsorption amount of CO_2 over the 1.18Na-FeMn (95/5) catalyst was larger than that of 1.20Na-Fe catalyst, due to the introduction of Mn. However, by further increasing the ratio of Mn in FeMn samples from 95/5 to 80/20, the adsorption amount of CO_2 gradually decreased because Mn species covered the adsorption sites of Fe species. The N_2 adsorption/desorption isotherms, the surface area, total pore volume, and average pore size of as-prepared catalysts were compared in Fig. S1 and Table S1 (Supporting Information). With the gradual increase of Mn content, these results did not change significantly. TEM images were displayed in Fig. S2 (Supporting Information). All catalysts presented similar morphologies and particle size distribution. The XPS spectra of as-prepared and spent catalysts were exhibited

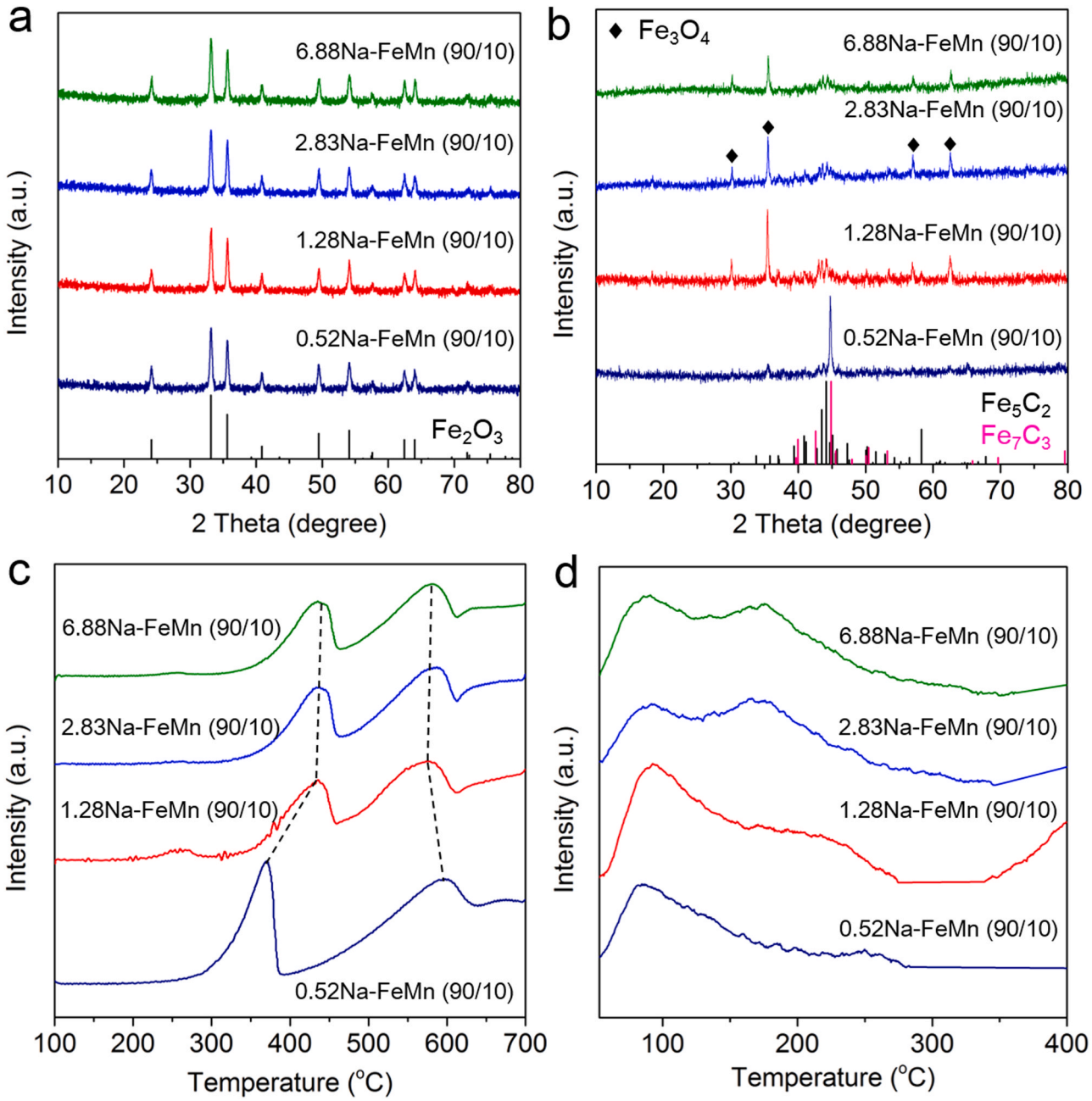

Fig. 2. (a) XRD patterns of as-prepared catalysts, (b) XRD patterns of spent catalysts, (c) H_2-TPR and (d) CO_2-TPD of nNa-FeMn (90/10) catalysts.

in Fig. S3 and S4 (Supporting Information), respectively. The phase compositions of different catalysts changed very little.

The XRD patterns of the as-prepared FeMn (90/10) catalysts with different Na loadings (0.52, 1.28, 2.83 and 6.88 wt%) were displayed in Fig. 2a. With increasing the loading of Na from 0.52 to 6.88 wt%, no peaks belonging to Na^+ species were detected due to the high dispersion of Na in FeMn catalyst system. The XRD patterns of the spent catalysts were shown in Fig. 2b. When the Na loading was 0.52 wt%, Fe_3O_4 and Fe_7C_3 (PDF#17–0333) phases were detected. However, with the further increase of Na loading, Fe_3O_4 and Fe_5C_2 were detected as the main phases rather than Fe_7C_3. The H_2-TPR profiles of the as-prepared catalysts were shown in Fig. 2c. Obviously, the reduction peak of Fe_2O_3 to Fe_3O_4 shifted to higher temperature with increasing the loading of Na. The results revealed that the Na inhibited the reduction of Fe oxides, which was consistent with the previous reports. [41] The CO_2-TPD profiles of the as-prepared FeMn (90/10) catalysts with different Na loadings were also presented in Fig. 2d. It is obvious that, with increasing the loading of Na from 0.52 to 2.83 wt%, the adsorption amount of CO_2 was significantly increased. By further increasing the loading of Na from 2.83 to 6.88 wt%, the adsorption amount of CO_2 remained stable generally.

3.2. Characterization of HZSM-5 and core-shell zeolites

The XRD patterns of HZSM-5 zeolites with different SiO_2/Al_2O_3 ratios were firstly compared in Fig. 3a. All samples exhibited the typical characteristic peaks of MFI structure. In Fig. 3b, the NH_3-TPD profiles of HZSM-5 zeolites displayed two apparent NH_3 desorption peaks at around 184 and 402 °C, which were assigned to the weak acid sites and the sum of medium and strong acid sites. With increasing SiO_2/Al_2O_3 ratio, the amounts of acid sharply decreased. It has been proved that the amounts of acid sites, especially Brønsted acid sites, are crucial for olefins to aromatics. [11,42–44] Therefore, the comparison and exploration of HZSM-5 zeolites with different SiO_2/Al_2O_3 ratios are very essential.

Fig. 4a showed XRD patterns of HZSM-5, HZSM-5@SiO_2, HZSM-5@S1-H, and HZSM-5@S1-S. As seen, the HZSM-5 zeolite and HZSM-5@SiO_2 core-shell zeolite displayed same characteristic peaks. HZSM-5@S1-H and HZSM-5@S1-S core-shell zeolites exhibited the same characteristic peaks of MFI structure, indicating the successful synthesis of the Silicalite-1 shell. On the other hand, XPS as a surface-sensitive technique was further employed to investigate the core-shell structure. The Al 2p XPS spectra of HZSM-5 and core-shell zeolites were shown in Fig. 4b. HZSM-5 zeolite showed a significant peak at 75.0 eV, which was associated with the presence of Al on the external surface. HZSM-5@SiO_2 core-shell zeolite exhibited a weak peak at 74.9 eV, representing that a small amount of Al was still detected on the external surface. This result implied that the amorphous SiO_2 shell via a conventional strategy was unable to completely cover the external surface. For HZSM-5@S1-H and HZSM-5@S1-S core-shell zeolites, no peak belonging to Al species was detected, indicating the successful construction of the HZSM-5@Silicalite-1 core-shell structure.

For HZSM-5@S1-H core-shell zeolite, during the hydrothermal synthesis process, in detail, a low alkalinity mother solution must be used to prevent the dissolution of aluminum in the HZSM-5 framework. However, the diluted solution also leads to the low yield and the production of a large amount of wastewater in turn. Compared with the traditional hydrothermal method, the solvent-free method not only successfully synthesized the zeolite with core-shell structure, but also significantly avoided the generation of wastewater. The N_2 sorption isotherms were listed in Fig. 4c, HZSM-5 and core-shell zeolites exhibited a sharp adsorption of N_2 at low pressure, suggesting these core-shell zeolites keeping the microporous structure. The surface area, pore size, and pore volume of HZSM-5 and core-shell zeolites were displayed in Table 1. ^{27}Al magic angle spinning (MAS) NMR spectra of HZSM-5 and core-shell zeolites were displayed in Fig. 4d. All zeolites exhibited a sharp band at 54 ppm, which was assigned to tetrahedrally coordinated aluminium. No peak belonging to octahedral extra-framework aluminium was detected. SEM images were recorded to obtain the surface morphology of these zeolites, as shown in Fig. 5. The original HZSM-5 zeolite had an approximately elliptical shape with a particle length around 4 μm. After coating amorphous SiO_2 shell, the shape and size of core-shell zeolite were almost unchanged, but the external surface became uneven and rough. For the HZSM-5@S1-H core-shell zeolite, it showed a regular hexagonal shape and the particle size increased to 7 μm. The HZSM-5@S1-S core-shell zeolite exhibited an elliptical shape, rough external surface and a large length around 12 μm. Compared with hydrothermal method, the solvent-free method was more conducive to synthesize large size core-shell zeolite due to absence of solvents. The results of distribution of Si element disclosed that, after coating HZSM-5 zeolite by SiO_2 or Silicalite-1 shell, the Si on the surface of all core-shell zeolites increased significantly. The EDS mapping further proved the successful synthesis of the core-shell structure.

In addition, given the crucial role of acidity on catalytic performance, overall acidic properties of original HZSM-5 and core-shell zeolites were characterized by NH_3-TPD, the Fourier-transform IR spectra of adsorbed pyridine (Py-FTIR) and di-tert-butyl-pyridine (DTBPy-FTIR) in details. Fig. 6a showed the NH_3-TPD profiles of HZSM-5 and core-shell zeolites. Compared with original HZSM-5 zeolite, the overall acidic amounts of core-shell zeolites were reduced with the introduction of

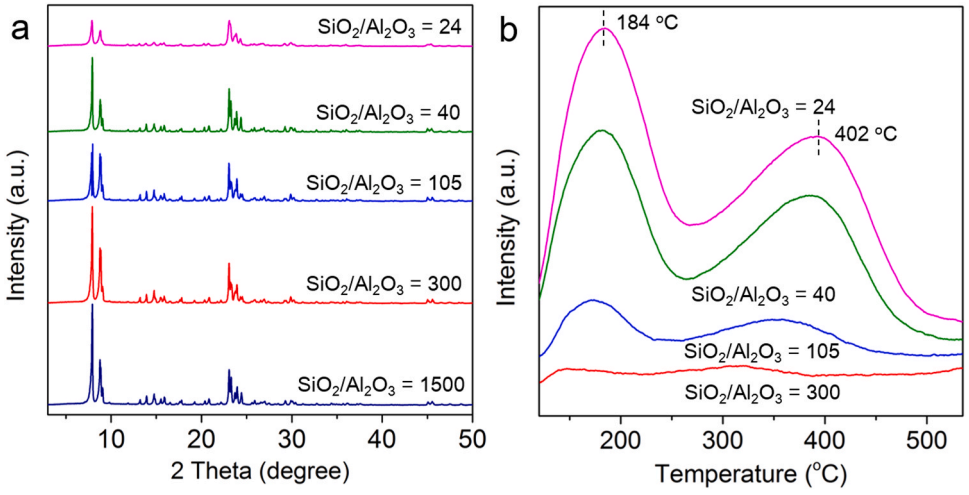

Fig. 3. (a) XRD patterns and (b) NH_3-TPD profiles of HZSM-5 zeolites with different SiO_2/Al_2O_3 ratios.

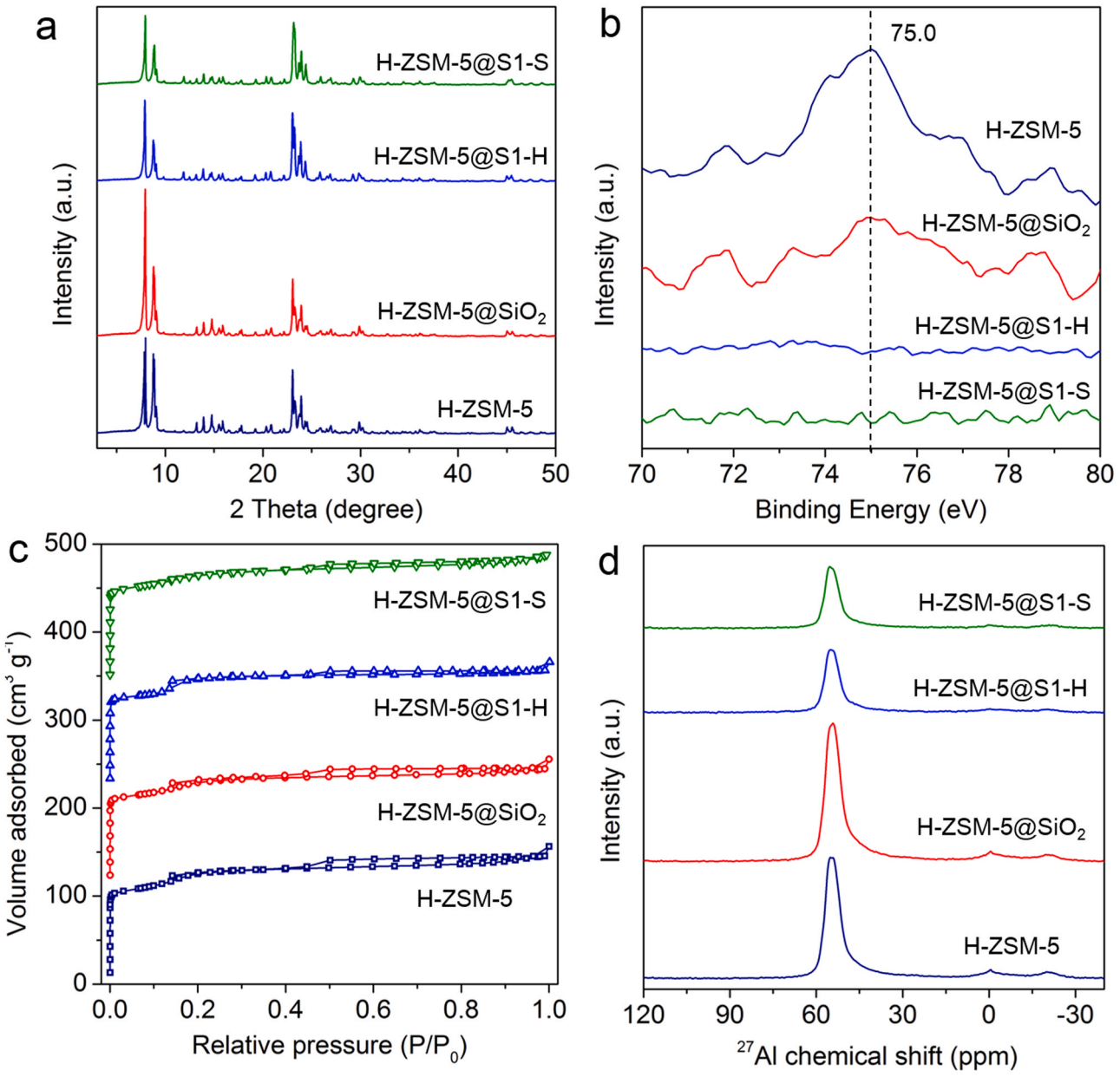

Fig. 4. (a) XRD patterns, (b) Al 2p XPS spectra, (c) N_2 adsorption/desorption isotherms and (d) ^{27}Al MAS NMR spectra of HZSM-5 and different core-shell zeolites.

Table 1
Texture and chemical properties of HZSM-5 and core-shell zeolites.

Sample	S_{BET} (m^2 g^{-1})[a]	D (nm)[b]	V (cm^3 g^{-1})[c]
HZSM-5	369	2.68	0.209
HZSM-5@SiO_2	341	2.62	0.189
HZSM-5@S1-H	372	2.31	0.193
HZSM-5@S1-S	366	3.01	0.213

[a] BET surface area.
[b] Pore size is obtained by BJH desorption.
[c] Pore volume is calculated by single point method.

non-acidic shell, because SiO_2 and Silicalite-1 shell covered the external surface acid sites. Clearly, Silicalite-1 shell covered more acid sites than amorphous SiO_2 shell. Py-FTIR experiments were carried out to identify the acid site types of the HZSM-5 and core-shell zeolites, as shown in Fig. 6b. The band at around 1452 and 1544 cm^{-1} were attributed to Lewis and Brønsted acid sites, respectively. It is obvious that, after coating SiO_2 or Silicalite-1 shell, Lewis acid sites were significantly reduced. Fig. 6c illustrated the DTBPy-FTIR spectra of HZSM-5 and core-shell zeolites to determine the external acid sites. The signal at 1616 cm^{-1} was assigned to the external surface acid sites. After coating HZSM-5 zeolite by SiO_2 shell, some external acid sites were still detected, indicating that SiO_2 shell did not completely cover all external acid sites. However, for HZSM-5@Silicalite-1 core-shell zeolites, no external acid sites were detected.

3.3. Effects of promoter loading on CO_2 hydrogenation performance

The effect of different Fe/Mn molar ratios on catalytic performances were compared in Fig. 7a and Table S2 (Supporting Information). In terms of 1.20Na-Fe sample, 28.4% CO_2 conversion, 19.2% CO selectivity, 34.7% light olefins selectivity, and 1.3% aromatics selectivity were obtained under the reaction conditions of 320 °C, 3 MPa, WHSV = 4000 mL g_{cat}^{-1} h^{-1}. By subsequently adding Mn in Fe catalysts, CH_4 and light paraffins selectivities slightly increased from 10.2% to 12.0% and 7.2% to 8.9%, respectively. By contrary, C_{5+} selectivity firstly

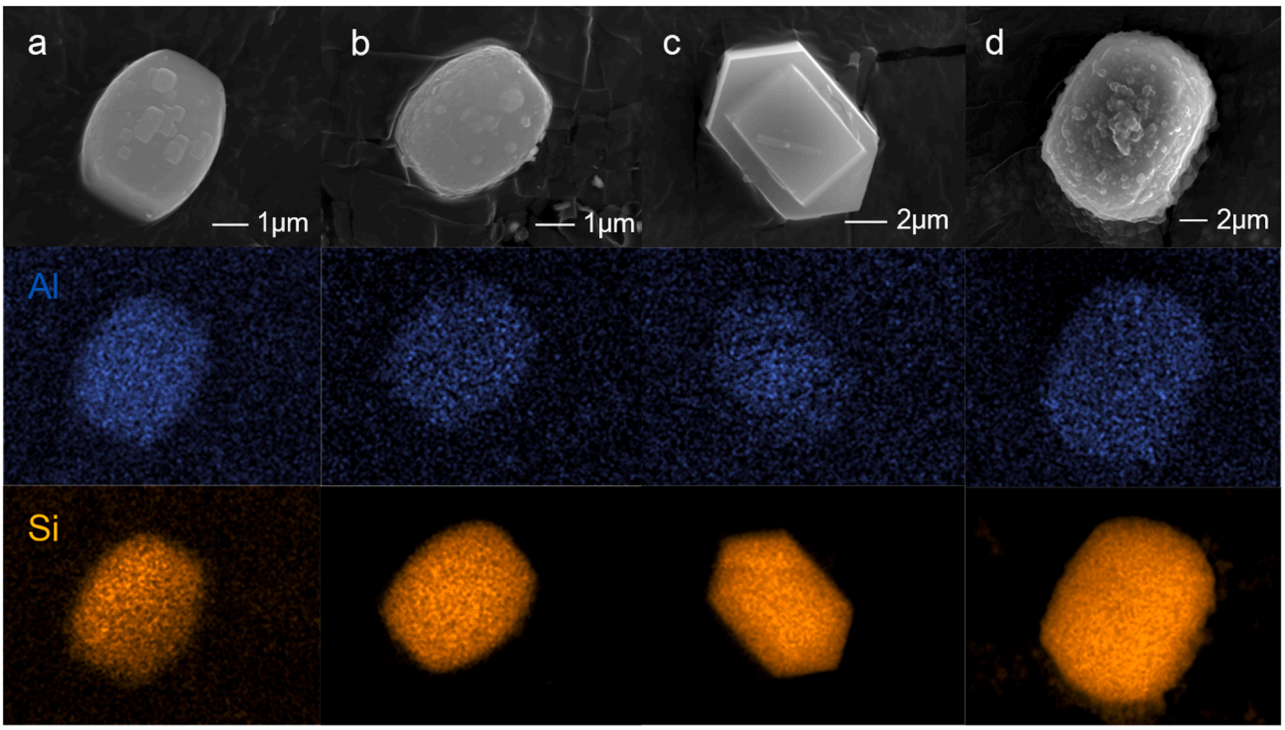

Fig. 5. SEM images of (a) HZSM-5, (b) HZSM-5@SiO_2, (c) HZSM-5@S1-H and (d) HZSM-5@S1-S core-shell zeolites and the EDS mapping of Al and Si.

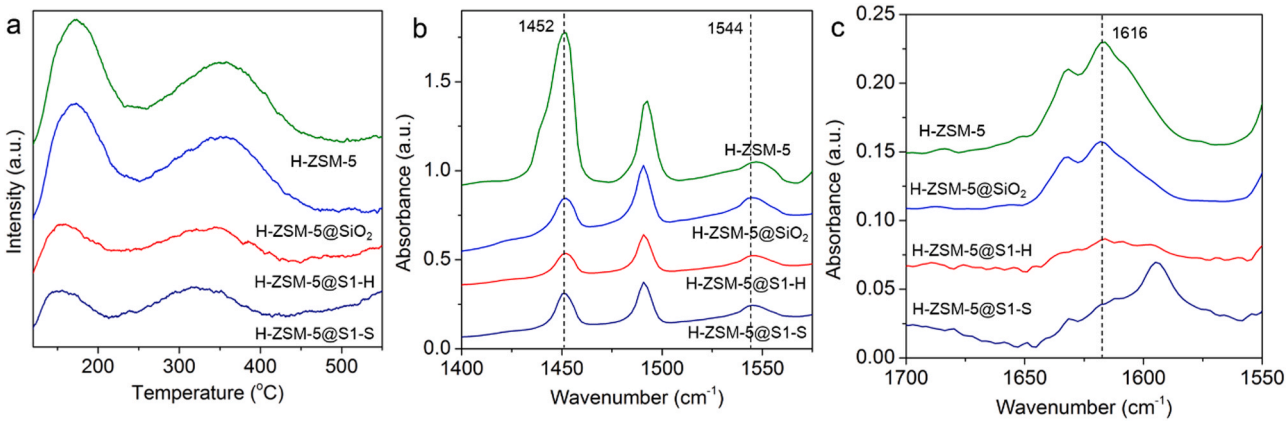

Fig. 6. (a) NH_3-TPD, (b) Py-FTIR and (c) DTBPy-FTIR spectra of HZSM-5 and different core-shell zeolites.

decreased from 46.6% to 39.5% and then increased to 42.3%. The light olefins selectivity firstly increased to 38.2% when Fe/Mn molar ratio was 90/10, and then decreased to 35.6%. In this process, CO_2 conversion, CO and aromatics selectivities remained stable generally. Although different amounts of Mn usage would affect performance, the product distribution of catalysts did not show significant differences in the experimental range. However, it is noteworthy that FeMn catalysts with a high content of Mn exhibited a high selectivity of light hydrocarbons. With the utilization of Mn promoter, the chain growth factors (α) slightly decreased compared to Na-Fe catalyst. These results indicated that the addition of Mn would slightly inhibited the chain-growth reactions and enhanced the light olefins selectivity [41,45]. Thus, for CO_2 hydrogenation to light olefins, the optimal Fe/Mn molar ratio was 90/10, under an approximate Na loading.

The impacts of different Na loadings in FeMn (Fe/Mn molar ratio was fixed to 90/10) catalysts for catalytic performances had also been investigated, as shown in Fig. 7b and Table S3 (Supporting Information). With the gradually increased Na loading from 0.52 to 6.88 wt%, CO_2 conversion firstly increased from 20.9% to 28.8% and then slightly decreased to 26.1%, while CO selectivity increased from 17.1% to 25.4%. However, CH_4 and light paraffins selectivities obviously decreased from 43.1% to 13.1% and 22.1% to 7.1%, respectively. The selectivity of light olefins firstly increased from 26.1% to 42.0% and then decreased to 40.7%, while C_{5+} selectivity increased from 8.7% to 39.5% and then slightly decreased to 38.3%. When the loading of Na was 0.52 wt%, the light olefins selectivity was lower than those of other catalysts with higher content of Na. This phenomenon could be ascribed to the weak promotional effects of Na promoter, in which high content of Na was beneficial to the formation of highly-active Fe_5C_2 phase rather than Fe_7C_3 (XRD pattern, Fig. 2b). When the loading of Na was 2.83 wt %, the light olefins selectivity reached 42.0%. However, excessive loading of Na had a negative effect for catalytic performance, which might be ascribed to the retarded reduction of iron species and coverage of active sites by Na promoter.

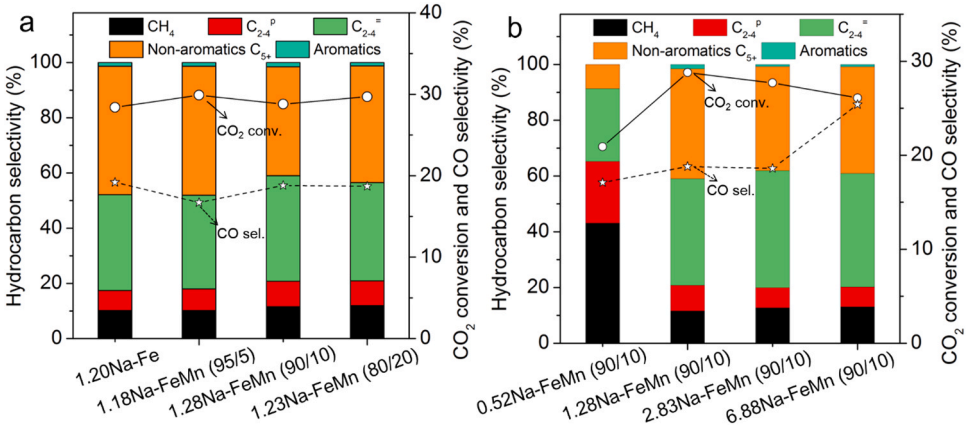

Fig. 7. Catalytic performances of nNa-FeMn (x/y) catalysts. CO_2 hydrogenation reaction conditions: 320 °C, 3.0 MPa, (25.7 vol% CO_2, 4.02 vol% Ar, and H_2 balance), WHSV = 4000 mL g_{cat}^{-1} h^{-1} and time on stream (TOS) = 8 h.

3.4. Effects of SiO_2/Al_2O_3 ratio on CO_2 hydrogenation performance

Fig. 8, Table S4 and S5 (Supporting Information) showed the results of composite catalysts for CO_2 hydrogenation, which contained 2.83Na-FeMn (Fe/Mn molar ratio was 90/10) catalyst and HZSM-5 zeolite with tunable SiO_2/Al_2O_3 ratio. Upon increasing the SiO_2/Al_2O_3 ratios of HZSM-5 zeolite, CO_2 conversion decreased from 28.1% to 22.7% and CO selectivity increased from 19.8% to 32.2%. CH_4 selectivity increased from 8.9% to 12.5%, while light paraffins selectivity decreased sharply from 19.1% to 7.5%. Light olefins selectivity firstly decreased from 18.2% to 13.0% and then increased to 42.5%. Aromatics selectivity was firstly increased from 33.1% to 36.5% and then decreased to 7.7%. It was significant that, after being combined with HZSM-5 zeolite, all samples exhibited high aromatics selectivities than blank 2.83Na-FeMn (90/10) catalyst. More apparently, the change trend of light olefins and aromatics selectivities were opposite, demonstrating that aromatics was formed from light olefins. On the other hand, for detailed aromatics distribution, with increasing the SiO_2/Al_2O_3 ratio of HZSM-5 zeolite from 24 to 1500, the PX selectivity firstly increased from 2.9% to 7.3% and then decreased to 0.3%. Similarly, PX/X ratio (the C-mol ratio of para-Xylene to all xylenes) firstly increased from 24.3% to 51.0% and then decreased to 15.7%. In addition, Benzene selectivity remained stable in these processes, at around 1%. By contrary, the selectivities of other light aromatics (Toluene, Ethylbenzene, ortho-Xylene and meta-Xylene) decreased with the increasing of SiO_2/Al_2O_3 ratio of HZSM-5 zeolite. At the same time, the heavy aromatics (C_{9+}) selectivity slightly increased from 10.4% to 13.3% and then decreased to 4.2%. As discussed above, light olefins could start aromatization reaction over the acid sites of zeolite, and the acid properties of zeolite presented a significant effect on catalytic performance. When the SiO_2/Al_2O_3 ratio was 105, aromatics selectivity reached 36.5%, while 7.3% PX selectivity and 51.0% PX/X ratio (the C-mol ratio of para-Xylene to all xylenes) were attained. In fact, high SiO_2/Al_2O_3 ratio of HZSM-5 zeolite did not have enough acid sites to aromatize olefins, thus the corresponding zeolite exhibited an inferior aromatics or PX selectivity. According to Fig. 8a, a low SiO_2/Al_2O_3 ratio of HZSM-5 zeolite was favorable to producing paraffins because hydrogen was transferred into unsaturated hydrocarbons, which was produced by aromatization process.

3.5. Effects of integration manners and iron/zeolite mass ratio on CO_2 hydrogenation

In order to enhance the PX/X ratio, HZSM-5@S1-S core-shell zeolite was directionally designed and replaced the conventional zeolite for CO_2 conversion to target PX. Firstly, the effects of different integration manners of 2.83Na-FeMn (90/10) and HZSM-5@S1-S core-shell zeolite were compared, and the catalytic performances were depicted in Fig. 9, Table S6 and S7 (Supporting Information). When Na-FeMn and HZSM-5@S1-S zeolite were separated in one reactor by a quartz stand layer, 5.4% aromatics selectivity and 44.4% PX/X ratio were obtained. After granule-mixing with quartz sand, aromatics selectivity and PX/X ratio increased to 14.2% and 70.8%, respectively. At the same time, only granule-mixing 2.83Na-FeMn (90/10) and HZSM-5@S1-S zeolite without quartz stand, aromatics selectivity further increased to 17.0% and PX/X ratio reached 75.4%. This was because olefins as the intermediates could efficiently diffuse to the micropores of HZSM-5@S1-S

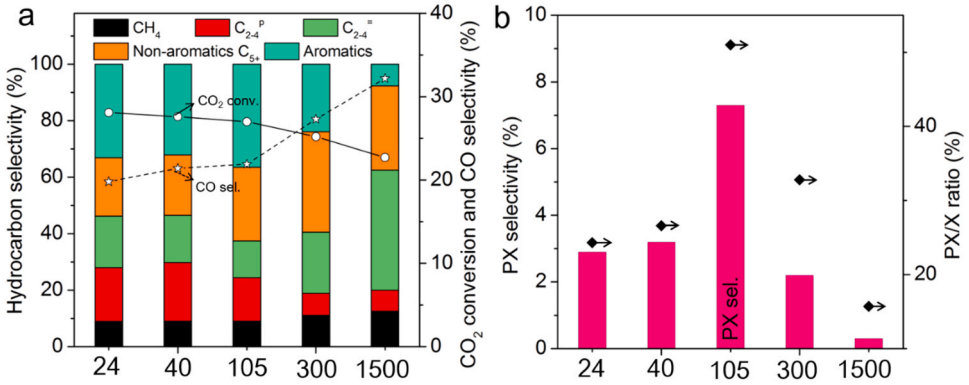

Fig. 8. Catalytic performances of 2.83Na-FeMn (90/10) composed HZSM-5 with different SiO_2/Al_2O_3 ratios, SiO_2/Al_2O_3 = 24, 40, 105, 300 and 1500. CO_2 hydrogenation reaction conditions: 320 °C, 3.0 MPa, (25.7 vol% CO_2, 4.02 vol% Ar, and H_2 balance), WHSV = 4000 mL g_{cat}^{-1} h^{-1} and time on stream (TOS) = 8 h, catalyst, iron/zeolite mass ratio = 1:1.

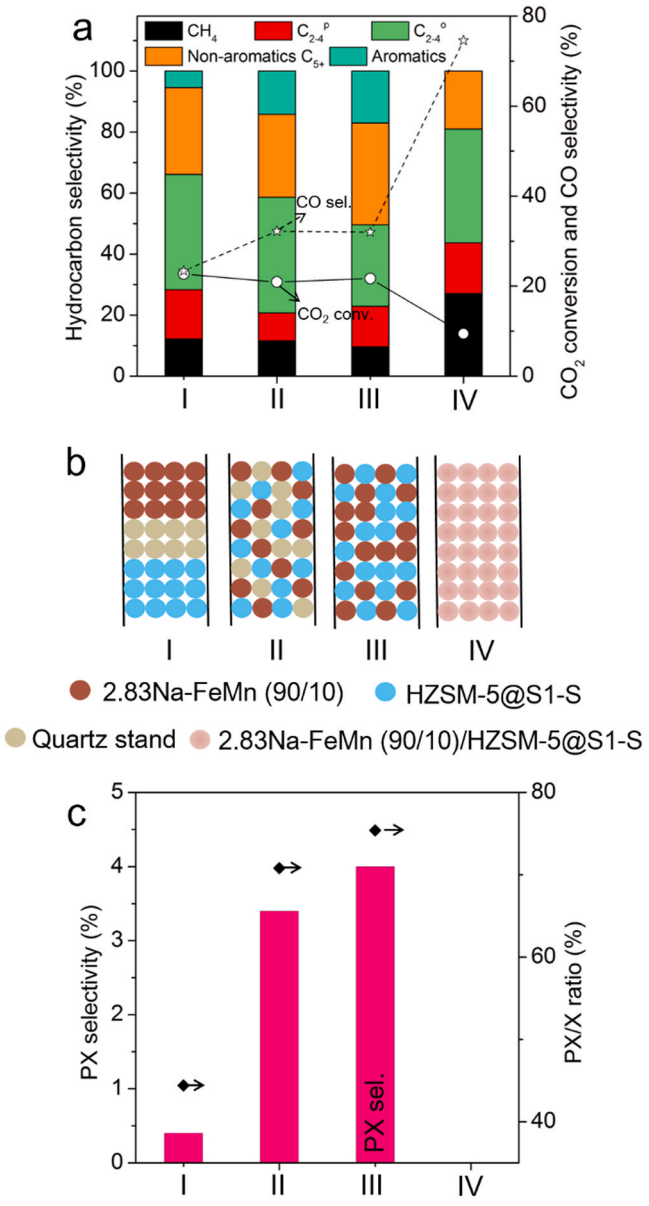

Fig. 9. Catalytic performances of 2.83Na-FeMn (90/10) and HZSM-5@S1-S with different integration manners. I, II, III and Ⅳ represent dual bed, granule-mixing with quartz sand, granule-mixing and powder-mixing, respectively. CO_2 hydrogenation reaction conditions: 320 °C, 3.0 MPa, (25.7 vol% CO_2, 4.02 vol% Ar and H_2 balance), WHSV = 4000 mL g_{cat}^{-1} h^{-1} and time on stream (TOS) = 8 h, catalyst, iron/zeolite mass ratio = 1:1.

zeolite (Fig. 9b, II and III). When 2.83Na-FeMn (90/10) and HZSM-5@S1-S zeolite were mixed by powder-mixing, the closest distance led to bad catalytic performance owing to the acid sites of zeolite were poisoned by the alkali sites of Na-FeMn catalyst [18]. It is worth mentioning that, when 2.83Na-FeMn (90/10) and HZSM-5@S1-S zeolite were integrated via granule-mixing manner, the selectivities of each component in aromatics were higher than those of other integration manners. These findings indicated that a closer distance was beneficial for the diffusion of light olefins, from Na-FeMn to HZSM-5@S1-S zeolite. As a result, aromatics selectivity was further increased, due to the aromatization reaction of light olefins on HZSM-5@S1-S zeolite. With the 2.83Na-FeMn (90/10) and HZSM-5@S1-S components brought closer to each other, PX selectivity was enhanced more significantly than OX and MX, due to the fact that the external surface of HZSM-5 zeolite was nonacidic silicalite-1 shell, and then the isomerization reaction of PX was limited. These results indicate that the integration manners of different active sites in Na-FeMn and HZSM-5@S1-S catalyst could significantly affect the distribution of hydrocarbons, and the granule-mixing manner was more beneficial for increasing aromatics selectivity and PX/X ratio.

Based on the discussion above, the effect of iron/zeolite mass ratio on catalytic performances were studied simultaneously, as shown in Fig. 10, Table S8 and S9 (Supporting Information). When the iron/zeolite mass ratio was adjusted from 1:1 to 1:3, CO_2 conversion decreased from 21.7% to 17.3%, CO selectivity increased from 32.0% to 36.9%. CH_4 and light paraffins selectivities were increased from 9.6% to 11.1% and 13.3% to 17.1%, respectively. The selectivity of aromatics increased from 17.0% to 24.7%. These results suggested that the higher mass ratio of zeolite/iron was beneficial for the aromatization of light olefins. Meanwhile, the selectivities of Toluene, Ethylbenzene, meta-Xylene and heavy aromatics increased. However, PX selectivity firstly increased from 4.0% to 7.5% and then decreased to 6.9%. Furthermore, 81.1% PX/X ratio was obtained at a mass ratio of 1:2 iron/zeolite. On the other hand, the light olefins selectivity decreased with boosting up the amount of core-shell zeolite, due to the fact that increasing total acid amounts of zeolite could effectively promote the conversion of light olefins to aromatics. However, further increasing the amount of core-shell zeolite in the composite catalyst (the iron/zeolite mass ratio from 1:2 to 1:3), PX/X ratio slightly decreased to 80.2%. Because increasing the amount of core-shell zeolite led to an increase of the total external surface of zeolite, the possibility for isomerization and alkylation of PX would increase. Therefore, the appropriate zeolite/iron mass ratio was efficient to increase PX/X ratio.

3.6. Comparison of different core-shell zeolites

Herein, HZSM-5@SiO_2 and HZSM-5@S1-H core-shell zeolites were employed to compare with HZSM-5@S1-S, as shown in Fig. 11, Table S10 and S11 (Supporting Information). As seen, with the utilization of core-shell zeolite catalysts with different synthesis strategies, the composite catalysts exhibited some differences. In detail, the HZSM-5@S1-S core-shell zeolite exhibited 7.5% PX selectivity, which was higher than HZSM-5@S1-H (7.0%) and HZSM-5@SiO_2 (6.9%) core-shell zeolites. The HZSM-5@SiO_2 showed 27.0% aromatics selectivity and 65.7% PX/X ratio, while the heavy aromatics selectivity reached 9.6%. The aromatics selectivity obtained from HZSM-5@SiO_2 was slightly higher than HZSM-5@S1-S (23.5%) and HZSM-5@S1-H (25.1%), due to the fact that total amounts of acid sites of HZSM-5@SiO_2 core-shell zeolite were more than those of HZSM-5@S1-S and HZSM-5@S1-H core-shell zeolites (NH_3-TPD profiles, Fig. 6a and Fig. 11). On the other hand, the PX/X ratio of HZSM-5@SiO_2 core-shell zeolite was lower than that of these core-shell zeolites, because the external surface acid sites were not completely covered by amorphous SiO_2 shell, which was consistent with the DTBPy-FTIR spectra (Fig. 6c). On the other hand, although HZSM-5@S1-S and HZSM-5@S1-H core-shell zeolites had the same Silicalite-1 shell, the HZSM-5@S1-S exhibited 81.1% PX/X ratio, and it was higher than that of HZSM-5@S1-H core-shell zeolite (78.6%). This was because the solvent-free method was more conductive to synthesize large particle size zeolite and the large-size core-shell zeolite was more favorable for increasing PX/X ratio (SEM imagines, Fig. 5). Meanwhile, the catalytic stability of 2.83Na-FeMn (90/10)/HZSM-5@S1-S was evaluated and the results were exhibited in Fig. S5 (Supporting Information). During 50 h, CO_2 conversion, PX and aromatics selectivities maintained stable, and the 2.83Na-FeMn (90/10)/HZSM-5@S1-S catalyst exhibited a good catalytic stability.

In addition, various strategies reported by different groups were used for synthesizing tailor-made zeolites with curtained acid properties, and the related zeolites were applied for CO_2 hydrogenation to aromatic. As summarized in Table S12 and S13 (Supporting Information), the bifunctional catalyst containing HZSM-5@S1-S exhibited a relatively excellent catalytic performance. These findings indicated that this

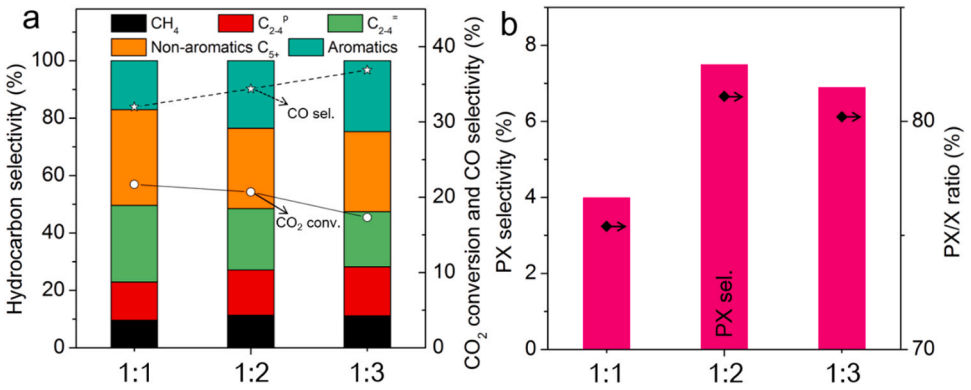

Fig. 10. Catalytic performances of 2.83Na-FeMn (90/10)/HZSM-5@S1-S with different iron/zeolite mass ratios (granule-mixing). CO_2 hydrogenation reaction conditions: 320 °C, 3.0 MPa, (25.7 vol% CO_2, 4.02 vol% Ar, and H_2 balance), WHSV = 4000 mL g_{cat}^{-1} h^{-1} and time on stream (TOS) = 8 h.

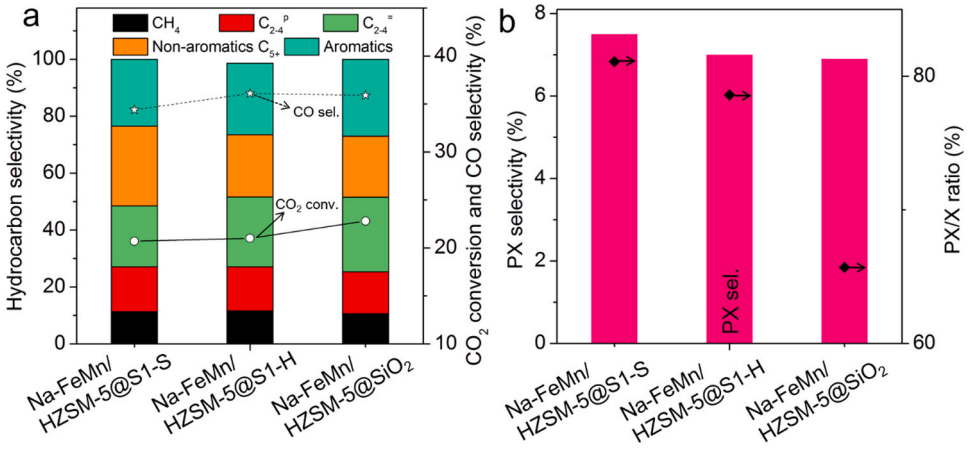

Fig. 11. Catalytic performances of 2.83Na-FeMn with different core-shell zeolites (granule-mixing). CO_2 hydrogenation reaction conditions: 320 °C, 3.0 MPa, (25.7 vol% CO_2, 4.02 vol% Ar, and H_2 balance), WHSV = 4000 mL g_{cat}^{-1} h^{-1} and time on stream (TOS) = 8 h, iron/zeolite mass ratio = 1:2.

solvent-free synthesis strategy has a good advantage for CO_2 hydrogenation to aromatic (or PX) via a modified Fischer-Tropsch synthesis route. At the same time, CO_2 hydrogenation reactions via methanol route with the assistance of different core-shell zeolites were evaluated (Table S14 and S15, Supporting Information). These results showed that the HZSM-5@S1-S core-shell zeolite still exhibited higher PX/X ratio than other conventional core-shell zeolites under the same reaction conditions. These findings suggested that the HZSM-5@S1-S core-shell zeolite also had good advantages for CO_2 hydrogenation through a methanol-assist route, and the solvent-free strategy was a promising tool for regulating acid properties of zeolite. As a consequence, the reported synthesis strategy could be used as an efficient reference for the preparation of zeolite with special surface acidity.

4. Conclusions

In summary, we prepared a composite Na-FeMn/HZSM-5@Silicalite-1 catalyst, which realized direct conversion of CO_2 to aromatics with high PX/X ratio. In this tandem catalysis system, CO_2 was firstly converted to CO and then CO was transformed to olefins over Na-FeMn catalyst, subsequently olefins was aromatized by HZSM-5@Silicalite-1 core-shell zeolite. For the Na-FeMn catalyst, a series of Fe/Mn molar ratios and different Na loadings were studied for CO_2 hydrogenation in detail. High light olefins selectivity (42.0%) was obtained, when the Fe/Mn molar ratio and Na loading were 90/10 and 2.83 wt%, respectively. Combining Na-FeMn and HZSM-5 zeolite, aromatics selectivity reached 36.5%. After coating Silicalite-1 shell on the external surface of HZSM-5 zeolite, PX/X ratio as high as 81.1% was obtained. The HZSM-5@Silicalite-1 core-shell zeolite was successfully synthesized by a solvent-free method, effectively hindering the PX alkylation and isomerization reaction on the external surface of zeolite. It is worth mentioning that the HZSM-5@Silicalite-1 zeolite also showed a higher PX/X ratio than other common core-shell zeolites. This works pave a new route for fabricating tailor-made core-shell zeolite with few surface acid sites, and constructing an efficient composite catalyst for catalyzing CO_2 hydrogenation into highly valuable PX.

CRediT authorship contribution statement

Weizhe Gao: Investigation, Data curation, Formal analysis, Writing – original draft. **Lisheng Guo:** Conceptualization, Data curation, Methodology, Project administration, Writing – review & editing. **Qinming Wu:** Data curation, Validation. **Chengwei Wang:** Data curation, Formal analysis. **Xiaoyu Guo:** Investigation, Validation. **Yingluo He:** Data curation, Investigation. **Peipei Zhang:** Formal analysis, Software. **Guohui Yang:** Software, Validation. **Guangbo Liu:** Formal analysis, Software. **Jinhu Wu:** Data curation, Validation. **Noritatsu Tsubaki:** Conceptualization, Data curation, Methodology, Resources, Project administration, Supervision, Writing – review & editing.

Declaration of Competing Interest

The authors declare that they have no known competing financial interests or personal relationships that could have appeared to influence the work reported in this paper.

Acknowledgements

NEDO project for carbon recycle and National Natural Science Foundation of China (22102001) are greatly appreciated.

Appendix A. Supporting information

Supplementary data associated with this article can be found in the online version at doi:10.1016/j.apcatb.2021.120906.

References

[1] C. Zhou, J. Shi, W. Zhou, K. Cheng, Q. Zhang, J. Kang, Y. Wang, Highly active ZnO-ZrO_2 aerogels integrated with H-ZSM-5 for aromatics synthesis from carbon dioxide, ACS Catal. 10 (2020) 302–310.

[2] Y. Wang, S. Kazumi, W. Gao, X. Gao, H. Li, X. Guo, Y. Yoneyama, G. Yang, N. Tsubaki, Direct conversion of CO_2 to aromatics with high yield via a modified Fischer-Tropsch synthesis pathway, Appl. Catal. B-Environ. 269 (2020), 118792.

[3] G. Song, M. Li, P. Yan, M.A. Nawaz, D. Liu, High conversion to aromatics via CO_2-FT over a CO-reduced Cu-Fe_2O_3 catalyst integrated with HZSM-5, ACS Catal. 10 (2020) 11268–11279.

[4] L. Guo, J. Li, Y. Zeng, R. Kosol, Y. Cui, N. Kodama, X. Guo, R. Prasert, V. Tharapong, G. Liu, J. Wu, G. Yang, Y. Yoneyama, N. Tsubaki, Heteroatom doped iron-based catalysts prepared by urea self-combustion method for efficient CO_2 hydrogenation, Fuel 276 (2020), 118102.

[5] P. Zhang, F. Han, J. Yan, X. Qiao, Q. Guan, W. Li, N-doped ordered mesoporous carbon (N-OMC) confined Fe_3O_4-FeCx heterojunction for efficient conversion of CO_2 to light olefins, Appl. Catal. B-Environ. 299 (2021), 120639.

[6] X. Cui, S. Chen, H. Yang, Y. Liu, H. Wang, H. Zhang, Y. Xue, G. Wang, Y. Niu, T. Deng, W. Fan, Improving methanol selectivity in CO_2 hydrogenation by tuning the distance of Cu on catalyst, Appl. Catal. B-Environ. 298 (2021), 120590.

[7] J. Zhang, S. Lu, X. Su, S. Fan, Q. Ma, T. Zhao, Selective formation of light olefins from CO_2 hydrogenation over Fe–Zn–K catalysts, J. CO2 Util. 12 (2015) 95–100.

[8] W. Gao, L. Guo, Y. Cui, G. Yang, Y. He, C. Zeng, A. Taguchi, T. Abe, Q. Ma, Y. Yoneyama, N. Tsubaki, Selective conversion of CO_2 into *para*-Xylene over a $ZnCr_2O_4$-ZSM-5 catalyst, ChemSusChem 13 (2020) 6541–6545.

[9] X. Zhao, W. Chen, G. Li, G. Feng, S. Li, X. Dong, Y. Song, X. Yu, X. Chen, W. Wei, Y. Sun, Gas-phase CO_2 photoreduction via iron/ZSM-5 composites, Appl. Catal. A-Gen. 595 (2020), 117503.

[10] G. Yang, Y. Kuwaharu, K. Mori, C. Louis, H. Yamashita, PdAg alloy nanoparticles encapsulated in N-doped microporous hollow carbon spheres for hydrogenation of CO_2 to formate, Appl. Catal. B-Environ. 283 (2021), 119628.

[11] J. Wei, R. Yao, Q. Ge, D. Xu, C. Fang, J. Zhang, H. Xu, J. Sun, Precisely regulating Brønsted acid sites to promote the synthesis of light aromatics via CO_2 hydrogenation, Appl. Catal. B-Environ. 283 (2021), 119648.

[12] F. Zeng, C. Mebrahtu, X. Xi, L. Liao, J. Ren, J. Xie, H.J. Heeres, R. Palkovits, Catalysts design for higher alcohols synthesis by CO_2 hydrogenation: trends and future perspectives, Appl. Catal. B-Environ. 291 (2021), 120073.

[13] R. Liu, Z. Ma, J.D. Sears, M. Juneau, M.L. Neidig, M.D. Porosoff, Identifying correlations in Fischer-Tropsch synthesis and CO_2 hydrogenation over Fe-based ZSM-5 catalysts, J. CO_2 Util. 41 (2020), 101290.

[14] X. Wang, D. Wu, J. Zhang, X. Gao, Q. Ma, S. Fan, T.S. Zhao, Highly selective conversion of CO_2 to light olefins via Fischer-Tropsch synthesis over stable layered K–Fe–Ti catalysts, Appl. Catal. A-Gen. 573 (2019) 32–40.

[15] Y. Xu, C. Shi, B. Liu, T. Wang, J. Zheng, W. Li, D. Liu, X. Liu, Selective production of aromatics from CO_2, Catal. Sci. Technol. 9 (2019) 593–610.

[16] Q. Yang, A. Skrypnik, A. Matvienko, H. Lund, M. Holena, E.V. Kondratenko, Revealing property-performance relationships for efficient CO_2 hydrogenation to higher hydrocarbons over Fe-based catalysts: statistical analysis of literature data and its experimental validation, Appl. Catal. B-Environ. 282 (2021), 119554.

[17] A.S. Skrypnik, Q. Yang, A.A. Matvienko, V.Y. Bychkov, Y.P. Tulenin, H. Lund, S. A. Petrov, R. Kraehnert, A. Arinchtein, J. Weiss, A. Brueckner, E.V. Kondratenko, Understanding reaction-induced restructuring of well-defined FexOyCz compositions and its effect on CO_2 hydrogenation, Appl. Catal. B-Environ. 291 (2021), 120121.

[18] J. Wei, Q. Ge, R. Yao, Z. Wen, C. Fang, L. Guo, H. Xu, J. Sun, Directly converting CO_2 into a gasoline fuel, Nat. Commun. 8 (2017) 15174.

[19] T. Numpilai, T. Witoon, N. Chanlek, W. Limphirat, G. Bonura, M. Chareonpanich, J. Limtrakul, Structure–activity relationships of Fe-Co/K-Al_2O_3 catalysts calcined at different temperatures for CO_2 hydrogenation to light olefins, Appl. Catal. A-Gen. 547 (2017) 219–229.

[20] R. Yao, J. Wei, Q. Ge, J. Xu, Y. Han, Q. Ma, H. Xu, J. Sun, Monometallic iron catalysts with synergistic Na and S for higher alcohols synthesis via CO_2 hydrogenation, Appl. Catal. B-Environ. 298 (2021), 120556.

[21] X. Liu, W. Zhou, Y. Yang, K. Cheng, J. Kang, L. Zhang, G. Zhang, X. Min, Q. Zhang, Y. Wang, Design of efficient bifunctional catalysts for direct conversion of syngas into lower olefins via methanol/dimethyl ether intermediates, Chem. Sci. 9 (2018) 4708–4718.

[22] Y. Shi, Q. Zhou, Z. Qin, Z. Wu, W. Jiao, M. Dong, W. Fan, J. Wang, Hierarchically structured Pt/K-Beta zeolites for the catalytic conversion of *n*-heptane to aromatics, Micro Mesopor. Mater. 324 (2021), 111308.

[23] B. Zhao, P. Zhai, P. Wang, J. Li, T. Li, M. Peng, M. Zhao, G. Hu, Y. Yang, Y.W. Li, Q. Zhang, W. Fan, D. Ma, Direct transformation of syngas to aromatics over Na-Zn-Fe_5C_2 and hierarchical HZSM-5 tandem catalysts, Chem 3 (2017) 323–333.

[24] P. Zhang, L. Tan, G. Yang, N. Tsubaki, One-pass selective conversion of syngas to *para*-xylene, Chem. Sci. 8 (2017) 7941–7946.

[25] I. Nezam, W. Zhou, G.S. Gusmão, M.J. Realff, Y. Wang, A.J. Medford, C.W. Jones, Direct aromatization of CO_2 via combined CO_2 hydrogenation and zeolite-based acid catalysis, J. CO_2 Util. 45 (2021), 101405.

[26] K. Cheng, W. Zhou, J. Kang, S. He, S. Shi, Q. Zhang, Y. Pan, W. Wen, Y. Wang, Bifunctional catalysts for one-step conversion of syngas into aromatics with excellent selectivity and stability, Chem 3 (2017) 334–347.

[27] T. Wang, C. Yang, P. Gao, S. Zhou, S. Li, H. Wang, Y. Sun, ZnZrOx integrated with chain-like nanocrystal HZSM-5 as efficient catalysts for aromatics synthesis from CO_2 hydrogenation, Appl. Catal. B-Environ. 286 (2021), 119929.

[28] S. Wang, T. Wu, J. Lin, J. Tian, Y. Ji, Y. Pei, S. Yan, M. Qiao, H. Xu, B. Zong, FeK on 3D graphene–zeolite tandem catalyst with high efficiency and versatility in direct CO_2 conversion to aromatics, ACS Sustain. Chem. Eng. 7 (2019) 17825–17833.

[29] A. Ramirez, A. Dutta Chowdhury, A. Dokania, P. Cnudde, M. Caglayan, I. Yarulina, E. Abou-Hamad, L. Gevers, S. Ould-Chikh, K. De Wispelaere, V.V. Speybroeck, J. Gascon, Effect of zeolite topology and reactor configuration on the direct conversion of CO_2 to light olefins and aromatics, ACS Catal. 9 (2019) 6320–6334.

[30] Y. Xu, T. Wang, C. Shi, B. Liu, F. Jiang, X. Liu, Experimental investigation on the two-sided effect of acidic HZSM-5 on the catalytic performance of composite fe-based fischer–tropsch catalysts and HZSM-5 zeolite in the production of aromatics from CO_2/H_2, Ind. Eng. Chem. Res. 59 (2020) 8581–8591.

[31] X. Cui, P. Gao, S. Li, C. Yang, Z. Liu, H. Wang, L. Zhong, Y. Sun, Selective production of aromatics directly from carbon dioxide hydrogenation, ACS Catal. 9 (2019) 3866–3876.

[32] Y. Wang, W. Gao, S. Kazumi, H. Li, G. Yang, N. Tsubaki, Direct and oriented conversion of CO_2 into value-added, Aromat., Chem. Eur. J. 25 (2019) 5149–5153.

[33] J. Zhang, W. Qian, C. Kong, F. Wei, Increasing *para*-Xylene selectivity in making aromatics from methanol with a surface-modified Zn/P/ZSM-5 catalyst, ACS Catal. 5 (2015) 2982–2988.

[34] K. Miyake, Y. Hirota, K. Ono, Y. Uchida, S. Tanaka, N. Nishiyama, Direct and selective conversion of methanol to *para*-xylene over Zn ion doped ZSM-5/silicalite-1 core-shell zeolite catalyst, J. Catal. 342 (2016) 63–66.

[35] Y. Wang, L. Tan, M. Tan, P. Zhang, Y. Fang, Y. Yoneyama, G. Yang, N. Tsubaki, Rationally designing bifunctional catalysts as an efficient strategy to boost CO_2 hydrogenation producing value-added aromatics, ACS Catal. 9 (2019) 895–901.

[36] Q. Wu, X. Meng, X. Gao, F.S. Xiao, Solvent-free synthesis of zeolites: mechanism and utility, Acc. Chem. Res. 51 (2018) 1396–1403.

[37] W. Gao, C.C. Amoo, G. Zhang, M. Javed, B. Mazonde, C. Lu, R. Yang, C. Xing, N. Tsubaki, Insight into solvent-free synthesis of MOR zeolite and its laboratory scale production, Micro Mesopor. Mater. 280 (2019) 187–194.

[38] J. Zhang, L. Wang, Z. Wu, H. Wang, C. Wang, S. Han, F.S. Xiao, Solvent-free synthesis of core–shell Zn/ZSM-5@Silicalite-1 catalyst for selective conversion of methanol to BTX aromatics, Ind. Eng. Chem. Res. 58 (2019) 15453–15458.

[39] Y. Jin, Q. Sun, G. Qi, C. Yang, J. Xu, F. Chen, X. Meng, F. Deng, F.S. Xiao, Solvent-free synthesis of silicoaluminophosphate zeolites, Angew. Chem. 52 (2013) 9172–9175.

[40] L. Ren, Q. Wu, C. Yang, L. Zhu, C. Li, P. Zhang, H. Zhang, X. Meng, F.S. Xiao, Solvent-free synthesis of zeolites from solid raw materials, J. Am. Chem. Soc. 134 (2012) 15173–15176.

[41] Y. Xu, P. Zhai, Y. Deng, J. Xie, X. Liu, S. Wang, D. Ma, Highly selective olefin production from CO_2 hydrogenation on iron catalysts: a subtle synergy between manganese and sodium additives, Angew. Chem. Int. Ed. 132 (2020) 21736–21744.

[42] Y. Xu, D. Liu, X. Liu, Conversion of syngas toward aromatics over hybrid Fe-based Fischer-Tropsch catalysts and HZSM-5 zeolites, Appl. Catal. A-Gen. 552 (2018) 168–183.

[43] K. Wang, S. Fan, J. Zhang, Q. Ma, W. Zhang, T.S. Zhao, Effects of synergy between Cr_2O_3 and hierarchical HZSM-5 on transformation of LPG toward propylene and ethylene, Fuel Process. Technol. 179 (2018) 53–59.

[44] K. Wang, J. Zhang, S. Fan, X. Peng, N. Tsubaki, T.S. Zhao, Transformation of LPG to light olefins on composite HZSM-5/SAPO-5, N. J. Chem. 45 (2021) 4860–4866.

[45] B. Liu, S. Geng, J. Zheng, X. Jia, F. Jiang, X. Liu, Unravelling the new roles of Na and Mn promoter in CO_2 hydrogenation over Fe_3O_4-based catalysts for enhanced selectivity to light α-Olefins, ChemCatChem 10 (2018) 4718–4732.